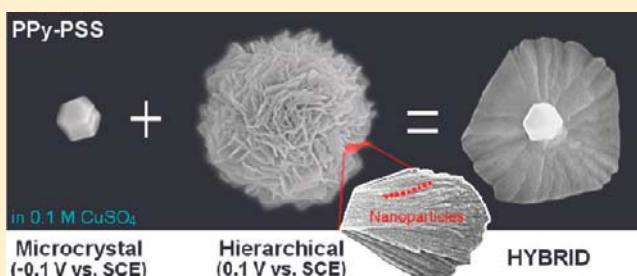# Electrochemical Fabrication of Copper-Based Hybrid Microstructures and Mechanism of Formation of Related Hierarchical Structures on Polypyrrole Films

Enrico Andreoli,* Valeria Annibaldi, Denise A. Rooney, and Carmel B. Breslin

Department of Chemistry, National University of Ireland Maynooth, Co. Kildare, Maynooth, Ireland

ABSTRACT: The surface electrochemistry of polypyrrole—polystyrene sulfonate (PPy—PSS) thin films is exploited for the fabrication of novel hybrid copper-based microstructures. The electrochemical deposition of the copper-based materials at the PPy—PSS film is strongly dependent on the electrode potential. This dependence is studied at three different potentials: 0.10, 0.00, and −0.10 V vs SCE. Hierarchical micro/nanostructures made of copper hydroxysulfate salts are only formed at 0.10 V vs SCE and are replaced with branched and single microcrystals of Cu_2O covered by a thin layer of $Cu(OH)_2$ at 0.00 and −0.10 V

vs SCE, respectively. The different structures can be coupled on the same film through a simple fabrication procedure to give hybrid microstructures. These novel hybrids consist of a central microcrystal (deposited at −0.10 V vs SCE) and a surrounding contour of welded nanosheets (deposited at 0.10 V vs SCE). The mechanism of nucleation and growth of the hierarchical micro/nanostructures formed at 0.10 V vs SCE is also reported. These structures are made from the assembly of nanoparticles into nanowires, nanosheets, and microclusters. These microclusters have a flowerlike shape within which each nanosheet forms a petal of the flower. The nucleation of the clusters is shown to be progressive.

◼ INTRODUCTION

The electrochemical fabrication of micro- and nanomaterials has been the object of various studies in recent years. In most cases the fabrication is performed through the electrochemical deposition of materials inside the voids of ordered porous templates. For example, the preparation of nanowire arrays made of different materials electrodeposited inside the porous structures of alumina membranes, nanochannel alumina, or anodic aluminum oxide.[1−5] Electrochemical fabrication can also be regarded as a building procedure whereby a deposit is constructed by combining materials electrochemically deposited in sequence. In one early study conducting polymers were electrodeposited in series to fabricate an organic p—n junction diode.[6] Polyaniline, for example, has been extensively used for the electrochemical fabrication of nanomaterials for a variety of applications.[7−10] Recently, photoactive oxide nanotubes and conducting polymers were electrodeposited in sequence to give a combined photoconductive material.[11] It is also interesting to report a reversed approach to fabrication called dealloying, a "corrosion-type" procedure which consists of etching an alloy made of two metals. One metal is electrochemically etched while the other one is passivated to form a nanoporous matrix.[12] These different strategies are all aimed at the same goal to obtain structured materials with micro- and nanostructure features.

Electrochemical deposition methods offer several advantages over other fabrication techniques as they are simple, cheap, and reproducible.[13] Furthermore, parameters such as the concentration of the electroactive species and the electrodeposition

potential have significant effects on the efficiency of the deposition and on the microstructure of the deposits.[13] In this paper we present results on the influence of the electrode potential on the shape and content of the microstructures deposited. Significantly, at certain applied potentials the microstructures are composed mainly of Cu_2O. Cu_2O has been extensively investigated for potential applications in different technologies including solar cells,[14,15] gas sensors,[16,17] and lithium batteries.[18,19] Its narrow band gap energy (1.9−2.2 eV), low material cost, and nontoxicity make Cu_2O a very promising material for photovoltaics.[20] Moreover, its conduction and valence bands are close to the reduction and oxidation potentials of water, respectively, enabling efficient water photolysis for hydrogen gas generation.[20] In recent years interest has developed on the shape controlled electrochemical deposition of Cu_2O microcrystals on a conducting substrate. These studies are important in order to enable any correlation of crystal shape with chemical and physical properties to be determined. Parameters that have been investigated which alter the shape of the Cu_2O crystal formed include surfactant molecule additives,[21] potential/current applied,[22] pH,[23] and the application of a magnetic field.[24,25] In this paper we show that by altering the electrode potential one can control the shape of Cu_2O microcrystals deposited on a conducting polymer. Moreover, we have prepared hybrid microstructures by

the sequential deposition of Cu_2O and then copper hydroxysulfates at different electrode potentials. To the best of our knowledge, this work is the first example of employing the electrode potential to control the electrochemical reactions of a conducting polymer film in order to alter the shape of Cu_2O microcrystals and fabricate copper-based hybrid microstructures.

Hierarchy in materials is related to the presence of structural elements organized at different scales.[26] Studies have shown that the size and shape of nanostructures have a significant effect on their properties and potential applications.[27,28] Electrodes coated with nanostructured metal and metal oxide layers have recently found application in a number of fields, including as anodes for fuel cells[29] or lithium batteries,[30] sensors,[31] optoelectronic devices,[32] and superhydrophobic surfaces.[33] A number of works have highlighted that the nanostructuring of metal or metal oxide electrodes can lead to enhanced electrical conductivity and better electrochemical activity.[29,30,32,34] Hierarchical flowerlike metal-based structures can result in superhydrophobic surfaces by increasing surface roughness.[35] It is interesting to note that hierarchical structures of copper sulfate hydroxide, which form part of the present work, have been shown to have superhydrophobic properties.[36]

The study of the mechanism of formation of the hierarchical structures can help identifying their elementary units and characterizing their assembling mode. The way the units combine with each other to form components of increasing dimensionality is useful, for example, in the scientific field of crystal growth and design. Also, as for the study of the mechanism of a chemical reaction, knowing which intermediates are involved in the growth of a structure should allow a better control of its properties and use. Previous work by our group has shown that copper-based hierarchical micro/nanostructures could be deposited on a polypyrrole—polystyrene sulfonate (PPy—PSS) film from aerated or oxygen-saturated $CuSO_4$ solutions at a potential of 0.10 V vs SCE.[37] The structures were fully characterized and found to consist of a mixture of two different copper hydroxysulfates ($[CuSO_4]_2[Cu(OH)_2]_3 \cdot 5H_2O$/ $CuSO_4[Cu(OH)_2]_3 \cdot H_2O$). It is relevant to note that these hierarchical micro/nanostructures could be used to form copper metal nanoparticles by electrochemical reduction, as reported in our recent paper.[38] Speculatively, the ease of conversion of hierarchical structures to nanoparticles might be related to the nature and assembling mechanism of their fundamental building units which are also nanoparticles.

The work outlined in this paper highlights how the subtle control of the interfacial processes of polypyrrole thin films can be used as a tool for the electrochemical deposition and fabrication of micro/nanomaterials. Furthermore, some interesting aspects related to the type of nucleation and the mechanism of growth of the hierarchical copper hydroxysulfate salts on PPy-PSS films are presented.

■ EXPERIMENTAL SECTION

Materials. The chemicals used in the present work were pyrrole (98%), poly(sodium 4-styrenesulfonate), M_w ~70 000 g/mol, and copper sulfate pentahydrate (99.999%). Water was distilled and Milli-Q purified in the laboratory (14 MΩ·cm, pH = 5.0). All chemicals were supplied by Sigma-Aldrich.

Preparations. A stock amount of pyrrole (Py) was vacuum-distilled and stored in the dark at −20 °C under nitrogen. The electropolymerizations were run in aqueous solutions made from fresh aliquots of distilled Py and poly(sodium 4-styrenesulfonate) (PSS). The molar concentration of the polyanion in solution was calculated from the molecular weight of the corresponding monomer unit. The PPy—PSS thin films were prepared on glassy carbon (GC, 0.126 cm^2) and gold (Au, 0.200 cm^2) electrodes using a standard three-electrode cell. The counter electrode was a platinum wire and the reference electrode a standard calomel electrode (SCE, all potentials in the figures are referred to SCE). The electrolyte solution was made of 0.15 M Py and 50 mM PSS dissolved in Milli-Q water. The polymer was grown at a constant potential of 0.60 V vs SCE to give uniform thin films. The electropolymerizations were stopped after a certain charge was reached, usually 40 mC/cm^2. The thickness of the PPy—PSS films was calculated as 120 nm using a volume-to-charge ratio of 3.00×10^{-4} cm^3/C.[39] The copper-based micro/nanostructures were formed electrochemically on the surface of the PPy—PSS films.[37] After the electropolymerization, the electrodes were thoroughly rinsed with Milli-Q water and immersed in 0.10 M $CuSO_4$ aerated or oxygen-saturated solution. The potential of the electrode was set at a constant value of 0.10 V vs SCE until a certain charge was passed (usually 40 mC/cm^2), and the copper-based structures were formed. Once the deposition was completed the working electrodes were extensively rinsed with Milli-Q water and left to dry. The same procedure as described above was applied for the fabrication of the copper-based microstructures, but at different potentials and for different time periods. A PPy—PSS film was freshly polymerized on the working electrode that was then rinsed and immersed in the copper sulfate solution. Three different potentials 0.10, 0.00, and −0.10 V vs SCE were applied to three different films. After the electrodeposition the electrodes were rinsed with Milli-Q water and characterized. Different copper-based structures were formed at each potential. In order to fabricate hybrid copper-based microstructures a step potential at −0.10 V vs SCE was applied to a new PPy—PSS film for a few seconds, followed by a prolonged deposition at 0.10 V vs SCE on the same film and in the same electrolyte solution.

Equipment. The electrochemical experiments were performed with a Solartron 1285 potentiostat. The electrochemical quartz crystal microbalance was a CH Instrument 400A equipped with a CH127 cell and CH125A gold crystal electrodes. The microscopy characterization was performed with a scanning electron microscope (SEM) Hitachi S-3200-N with a tungsten filament electron source equipped with an Oxford Instrument INCAx-act EDX system. Another SEM was available at the Tyndall National Institute (Cork, Ireland), a Hitachi S-4000 with a cold cathode field emission electron source (FE-SEM) equipped with Princeton Gamma Technology Avalon 8000 EDX system. The samples were sputter-coated with gold or gold/palladium ultrathin films with an AGAR automatic sputter coater equipped with an AGAR terminating film thickness monitor unit. The X-ray photoelectron spectroscopy (XPS) equipment was a Kratos Axis 165 equipped with a monochromatic Al source (Kα 1486.58 eV) with a spot size of 1 mm. The source power was 150 W (10 mA, 15 kV), the takeoff angle was set normal to the sample surface, the construction and peak fitting in the narrow region spectra were performed using a Shirley type background, and the synthetic peaks were of a mixed Gaussian—Lorentzian type. Adventitious carbon was used for charge reference; the C 1s line of adventitious hydrocarbon was assumed to have a binding energy of 284.8 eV.
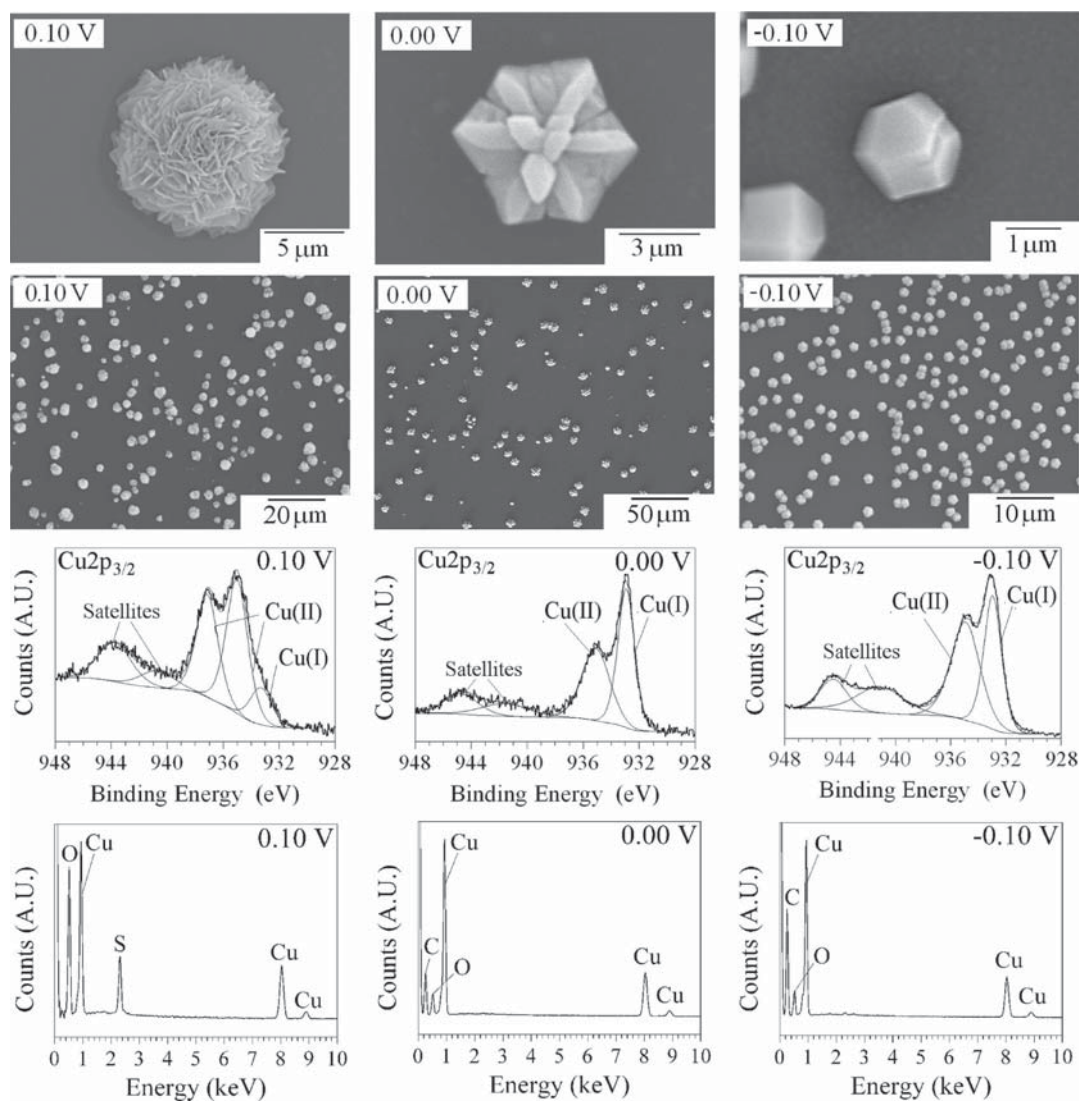
Figure 1. SEM micrographs and corresponding XPS Cu $2p_{3/2}$ and EDX spectra of copper-based materials deposited on PPy—PSS films at 0.10, 0.00, and −0.10 V vs SCE from aerated or oxygen-saturated 0.10 M CuSO$_4$ to a total charge of 40 mC/cm^2. The XPS Cu $2p_{3/2}$ signals are fitted to show the corresponding contribution of Cu(I) and Cu(II) with its satellites peaks. The main EDX peaks are assigned to copper, sulfur, and oxygen. The carbon peak is due to the polymer film and electrode present underneath the deposits.

■ RESULTS AND DISCUSSION

Fabrication of Copper-Based Hybrid Microstructures. The electrochemical deposition of copper-based materials at PPy—PSS thin films is strongly dependent on the electrode potential. While the deposition at 0.10 V vs SCE gives the formation of hierarchical copper hydroxysulfates micro/nanostructures,[37] the copper electrodeposits formed at lower potentials could possibly contain any or a mixture of copper metal, copper oxides, hydroxides, and/or hydroxysulfates. In order to investigate the influence of deposition potential on the nature of the structures, the modified films were characterized using SEM-EDX and XPS after electrodeposition at three potentials (Figure 1). The first striking observation is the variation in the shape of the materials with the decrease of deposition potential. The hierarchical copper-based micro/nanostructures are only formed at 0.10 V vs SCE. These are replaced with branched microcrystals at 0.00 V vs SCE and single

microcrystals at −0.10 V vs SCE. In all cases the surface of the electrodes is covered by an even distribution of deposited material as shown by the lower magnification micrographs of Figure 1. The composition is also dependent on the electrode potential. The EDX spectra show the presence of sulfur only in the micro/nanostructures; hence, at deposition potentials of 0.00 and −0.10 V vs SCE the crystals are made up of copper hydroxide/oxides. XPS spectra were taken in order to establish which of these components are present in the deposits. The Cu $2p_{3/2}$ signals and their respective fittings are given in Figure 1. The XPS spectrum of the hierarchical structures has been discussed in detail previously,[37] and it is reported again here for completeness. The deposits formed at 0.00 and −0.10 V vs SCE both show a peak at 932.9 eV which is related to either copper metal or Cu$_2$O (the peak of CuO is found at higher binding energy, e. g., 933.8 eV).[40] The Pourbaix diagram of copper[41] predicts that at potentials of deposition of 0.00 and −0.10 V vs SCE copper metal can only form at pH below 4 and 6, respectively.
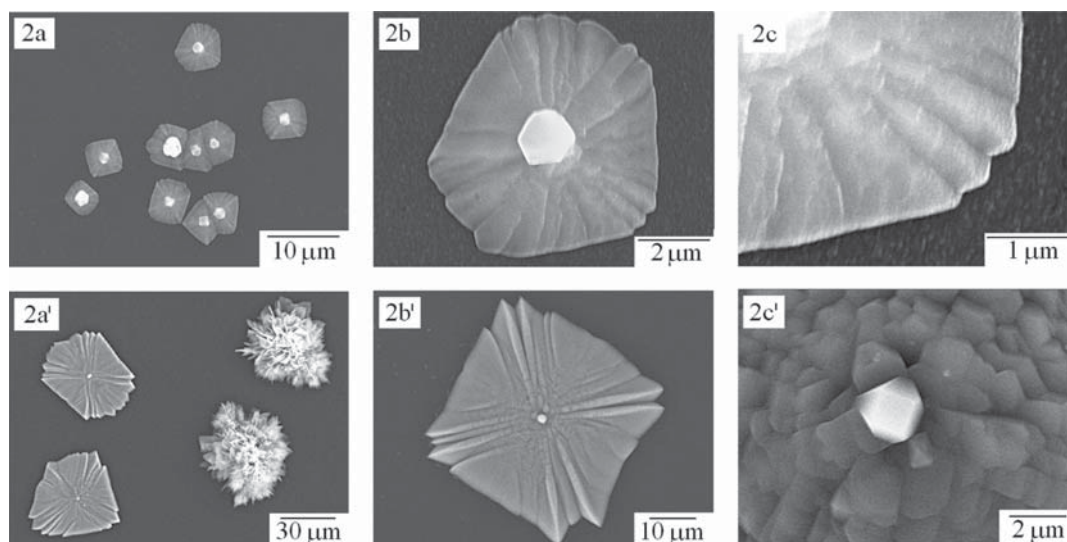
Figure 2. Hybrid copper-based microstructures electrodeposited on PPy−PSS thin films from aerated 0.10 M CuSO$_4$ after a pulse at −0.10 V vs SCE for 10 s followed by a deposition at 0.10 V vs SCE for a total charge of 40 mC/cm^2 (2a, 2b, 2c) and 400 mC/cm^2 (2a′, 2b′, 2c′).

Reasonably, the pH at the film surface is much higher during the electrodeposition because of OH$^-$ generation from the reduction of oxygen.[37] It follows that for both the deposits formed at 0.00 and −0.10 V vs SCE the peak at 932.9 eV is due to the presence of Cu$_2$O and not of copper metal. In addition to the peak at 932.9 eV, the Cu 2p$_{3/2}$ spectra recorded for the deposits formed at 0.00 and −0.10 V vs SCE showed peaks at 935.1 and 934.9 eV, respectively, which are typical of Cu(OH)$_2$ with its corresponding satellite peaks.[42] Considering that XPS probes the top 10 nm of the sample surface, a very thin layer of Cu(OH)$_2$ must be present on the deposits surface. The Cu 2p$_{3/2}$ signals observed from the deposits formed at 0.00 and −0.10 V are nearly identical to those reported by Yin et al. for Cu$_2$O nanocrystals.[43] The only difference is that such nanocrystals were covered by an amorphous layer of CuO. The surface characterization data are consistent with the deposits formed at 0.00 and −0.10 V versus SCE being composed of Cu$_2$O covered by a thin layer of Cu(OH)$_2$. The shapes of these microcrystals are also in agreement with those observed for the electrochemical deposition of Cu$_2$O.[22] In particular, the deposit formed at −0.10 V vs SCE has the shape of cubic truncated pyramids, which is characteristic of Cu$_2$O crystals in the case of similar growth rates along the ⟨100⟩ and ⟨111⟩ directions.[44,45] The electrodeposition of Cu$_2$O materials has been receiving much attention in the past few years because of their application, for example, in homo- and heterojunction solar cells.[46−49] In general, these materials are all potentially very interesting; in fact, micro- and nanomaterials of copper hydroxide and/or oxides have been considered in various fields of application such as sensing, solar energy harvesting, and catalysis.[43,50−52]

The electrochemical deposition of various copper materials and structures at the PPy−PSS films is possible because of the different processes involved at the film surface, such as oxygen reduction and diffusion of ions through the film.[37] These processes are in simultaneous competition, and the outcome of the electrodeposition is dependent on their relative rates. These rates can be altered by changing the electrode potential, implying that a reaction can be excluded through the application of an appropriate potential. In the present case this reaction is the electrocrystallization of hydroxysulfate species which is dominant at 0.10 V vs SCE, but excluded below 0.00 V vs SCE. The same consideration is true if the potentials are applied in the opposite direction. For example, if the first potential applied to the polymer film was −0.10 V vs SCE, the deposited species would be single microcrystals, but then at 0.10 V vs SCE the deposited species would become hierarchical micro/nanostructures, all on the same electrode modified surface. This would provide the means of coupling the two structures to form hybrids. Accordingly, the electrochemical deposition of hybrid copper-based microstructures was performed on PPy−PSS films by applying first a short potential pulse at −0.10 V vs SCE, followed by a longer deposition at 0.10 V vs SCE. The resulting structures are shown in Figure 2.

The structures, as expected, are made of two components. The central component is a microcrystal, whereas the surrounding material is a contour of welded sheets. Micrograph 2a shows a group of hybrids that are mostly of similar size and shape, with each microcrystal evenly adorned. Micrographs 2b and 2c show the details of the welded sheets that are concentrically distributed around the microcrystal. The hybrids in 2a′, 2b′, and 2c′ are larger versions of the ones shown in 2a, 2b, and 2c, as they were deposited for a considerably longer period of time at 0.10 V vs SCE (400 mC/cm^2 compared to 40 mC/cm^2). Interestingly, the central microcrystal does not increase in size with continued deposition at 0.10 V vs SCE, but the surrounding welded segment increases considerably to give hybrid dimensions as wide as 50 μm (diagonal). Moreover, as shown from a comparison of micrographs 2c and 2c′, the surface morphology of the welded structure becomes rougher with increasing deposition periods. Also, for long deposition periods the formation of additional and independent hierarchical micro/nanostructures is observed on the film, as shown in micrograph 2a′. The flat and welded appearance of the hybrids, instead of being made from clusters of individual nanothin sheets, as formed previously at this potential (Figure 1), is likely to be due to a seeding effect of the central microcrystals.[53] These crystals may act as seeds for the nucleation of the copper hydroxysulfates sheets that expand flat

20079

dx.doi.org/10.1021/jp204092x |*J. Phys. Chem. C* 2011, 115, 20076–20083

from the center onto the film surface, rather than growing into a hierarchical micro/nanostructure. Discrete hybrids are formed, but as evident from micrograph 2a, if the initial microcrystal nucleation sites are not sufficiently far apart, the hybrids can merge to give more complex structures. The electrodeposition of the hybrids is reproducible, and as observed earlier for each of the separate electroforms, the micro-hybrids are distributed across the entire polymer film surface (Figure 3).

The variety of structures formed upon a 200 mV change of potential is remarkable evidence of the diverse processes involved at the film/solution interface during the electrochemical depositions. The efficient nucleation of the copper deposits is enhanced by the high localized surface concentration of captured Cu^{2+} ions.[16] However, other simultaneous interfacial reactions determine the shape and composition of the deposits. At 0.10 V vs SCE, the deposition is governed by the presence of sulfate and hydroxide ions from the electrolyte solution and the oxygen reduction reaction, respectively.[37] At the lower potentials of 0.00
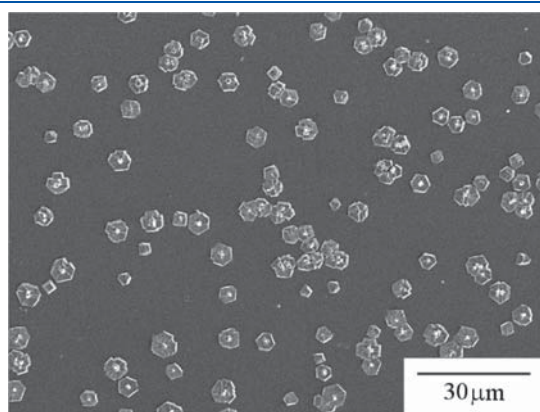

Figure 3. SEM micrograph of the copper-based hybrid micro/nanostructures formed on the PPy—PSS films as described in Figure 2 for a total charge of 40 mC/cm^2.

and −0.10 V vs SCE, the reduction of oxygen occurs at a higher rate, leading to the pH increase necessary for deposition of structures composed of copper hydroxide/oxides.

Formation of Copper Hydroxysulfates Hierarchical Structures. In order to gain a greater understanding of the means of formation of the structures on the polymer surface, an investigation was carried out on the mechanism of formation of the copper hydroxysulfates hierarchical micro/nanostructures. The means of preparation and characterization of these structures has been discussed elsewhere.[37] In order to investigate the mechanism of nucleation and growth, SEM micrographs of the structures were recorded at different stages of growth (Figure 4). The micrographs shown, designated as 4a—4a′, 4b—4b′, and 4c—4c′, represent the evolution of the structure as a function of time. At the very early stages (4a) a bone-shaped copper-based stick is observed, and it appears to sit on top of the polymer film; the size of the stick is about 3 μm long and 1 μm wide. At this stage, the stick is already made of several layers, a few tens of nanometers thick. Copper-based nanoparticles of about 20−50 nm are seen aligned along the length of the stick, forming numerous nano-wires (4a′). With the progression of the electrodeposition, other sticks, similar to the first one, are formed to give an almost centered structure (4b). At this stage, the sticks are still made of nanowire/nanoparticles (4b′). Once the structure become larger, it resembles the final flowerlike hierarchical shape (4c) and nanowire ends can still be seen at the edge of the sticks (4c′). At this stage, the flowers are made up of sticks, with each stick assembling to give what could be described as a petal of a flower. By the end of the electrodeposition, a cluster of compact petals is formed.[37] At the beginning of the flower formation (4a), the nanoparticles are likely to nucleate directly on the film surface, most probably from the Cu^{2+} ions that are captured and aligned along the polymer chains of the film. This assumption is based on the work by Yang et al.[54] in which it is shown that thin films of PPy—PSS (30−60 nm) are made of polymer chains lying parallel to each other on the electrode surface. Other nanoparticles are then crystallized at the same site, causing the formation of nanowires that extend to give the growth of nanosheets. Until
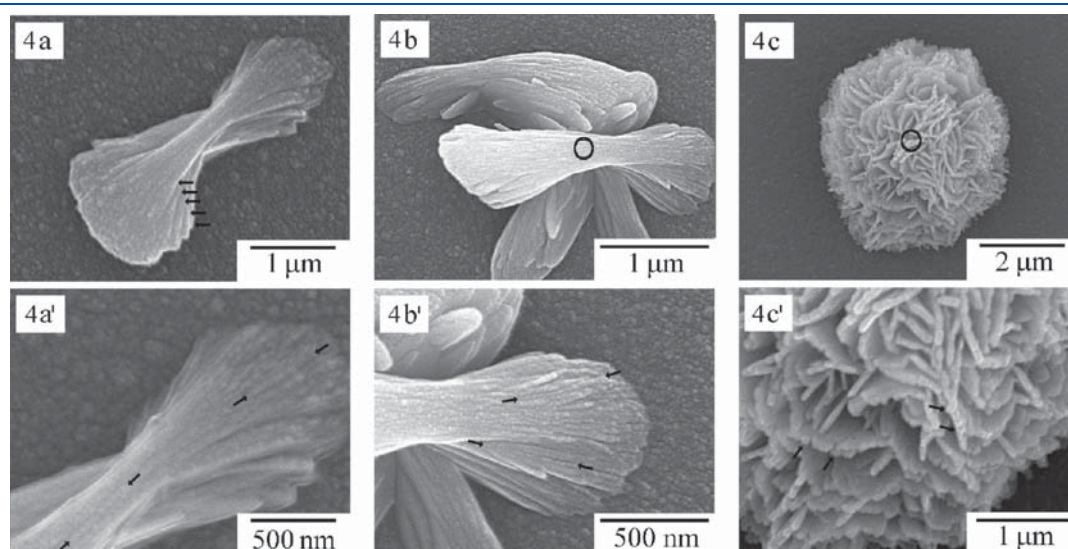
Figure 4. SEM micrographs showing the stages of formation of hierarchical copper-based micro/nanostructures on a PPy—PSS film after deposition from aerated 0.10 M CuSO$_4$ at 0.10 V vs SCE. The deposition time increases from left to right. The structures in the first row are shown enlarged in the second row. The arrows and circles are used to highlight the main features of the structures.
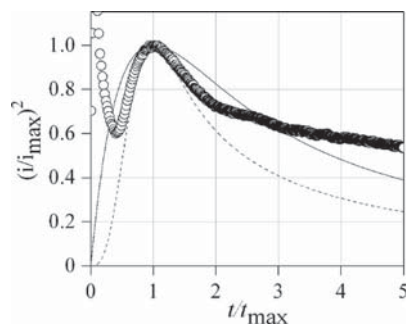
Figure 5. Dimensionless plot of the current–time response for the deposition of hierarchical copper-based micro/nanostructures onto a PPy–PSS film from an oxygen-saturated solution of 0.10 M CuSO$_4$ at 0.10 V vs SCE. The solid and dashed lines are the profiles for instantaneous and progressive nucleation, respectively, from the Scharifker–Hills model.
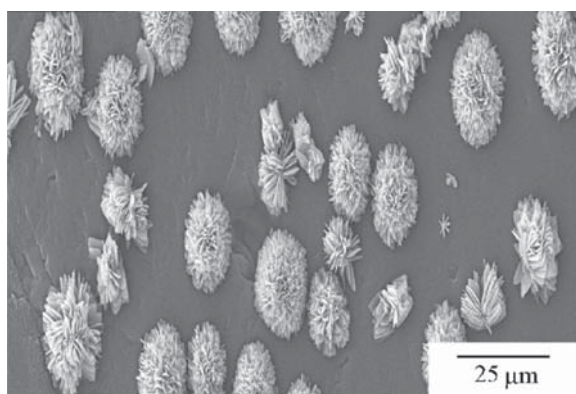

Figure 6. SEM micrograph of the hierarchical copper-based micro/nanostructures formed on the PPy–PSS films in aerated 0.10 M CuSO$_4$ at 0.10 V vs SCE. The overall charge of deposition is 80 mC/cm^2.

this point, the deposition process is governed by the electrochemistry of the polymer surface with the consequent nucleation and growth of the first group of petals. In the meantime, the nanoparticles grow in diameter forming thicker sheets with jagged borders. Eventually, smooth petals are formed with no particles visible at the petal edges in the finished flowers.[37] During this part of the growth, the copper hydroxysulfates are likely to be deposited directly on the already formed petals and not at the film.

The potentiostatic deposition of three-dimensional structures from multiple nucleation sites in the diffusion-controlled regime is described by the Scharifker–Hills model.[55] According to this model, two diagnostic relationships can be used to determine whether the nucleation of the copper-based micro/nanostructures is instantaneous or progressive. In order to compare the experimental data to the model equations, the current–time data are plotted in the dimensionless coordinates $(i/i_{MAX})^2$ and t/t_{MAX}, where i_{MAX} is the current maximum of the chronoamperometric response reached at time t_{MAX}. In the present case $t_{MAX} = 195$ s and $i_{MAX} = -0.171$ mA/cm^2, and the resulting curve is shown in Figure 5. The solid and dashed lines represent the dimensionless profiles of instantaneous and progressive nucleation, respectively.

At the start of the nucleation, corresponding to the minimum of the current–time response just above $^1/_2 t_{MAX}$, the
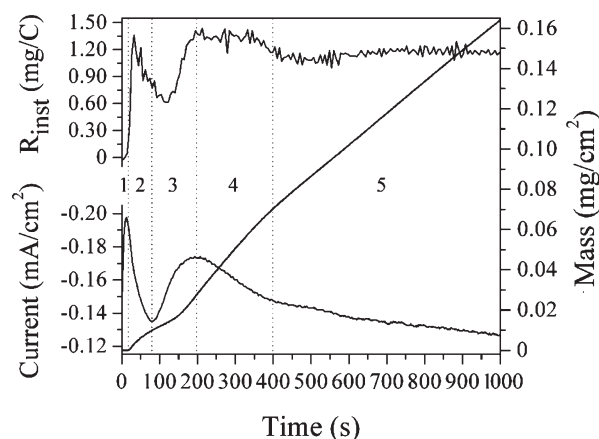
Figure 7. Current, mass, and instantaneous mass-to-charge ratio for the electrodeposition of hierarchical copper-based micro/nanostructures formed on a PPy–PSS film form oxygen-saturated 0.10 M CuSO$_4$ at 0.10 V vs SCE.

experimental data follow closely the model of progressive nucleation. The same is true around the current maximum at t_{MAX}. This part of the current profile is typical of depositions in which the formation of new nuclei is faster than the growth of existing nuclei;[55] the result is the progressive superposition of the currents of formation and growth of each nucleus. The data start departing from both models at about $2t_{MAX}$ as a result of the changes in the deposition process, such as precipitation from the solution rather than direct nucleation on the film surface or changes of pH and composition of the solution during the deposition.[56] In addition, the progressive nucleation is also evident from Figure 6, where a large number of nucleation sites is found, with each hierarchical structure growing in an independent manner. The structures have different sizes, confirming that the nucleation is progressive, with new sites being established during the electrodeposition period.

The mechanism of formation of the hierarchical structures can also be analyzed by comparing current, mass, and mass-to-charge ratios during the electrochemical deposition. The mass-to-charge ratio, R, is the mass deposited per unit of charge and is proportional to the molar mass, M, of the deposited material $(R = M/nF)$. The ratio is calculated from the slope of the mass–charge curve. The value of the ratio at each single time of the deposition is labeled as the instantaneous ratio, R_{inst}. The electrodeposition of the hierarchical copper-based micro/nanostructures can be divided into five stages, as shown in Figure 7. A scheme of the mechanism is also given in Figure 8. In the first stage there is an increase of current without any significant amount of deposited mass; consequently, the R_{inst} is close to zero. This stage lasts less than 20 s. The charge passed during this stage is used to reduce either oxygen or the polymer film. A current maximum is then reached and this is followed by a decrease in the current, but in contrast to the previous stage there is a correlated increase in mass. This second stage lasts about 60 s and is mainly due to the capture of Cu^{2+} ions by the polymer film. The third stage corresponds to an increase in current and extends from about 75 to 200 s. This is the current associated with the nucleation of hierarchical structures which are isolated from each other. Additionally, during the first 200 s of the experiment the mass begins to increase and R_{inst} climbs toward its first plateau value. On close inspection of Figure 7, it can be seen that the mass
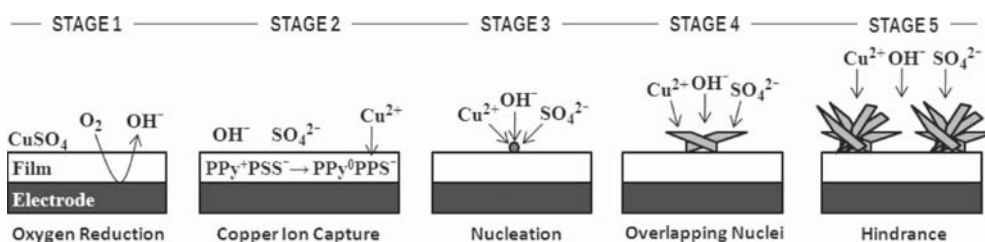
Figure 8. Simplified representation of the mechanism of formation of copper-based hierarchical micro/nanostructures.

increase lags behind the current increase, so that the increase in R_{inst} does not mirror exactly the increase in current. This is related to the fact that part of the charge consumed is connected with the reduction of dissolved oxygen and the generation of hydroxide ions.[37] When the concentrations of Cu^{2+} and OH^- ions have reached a critical value, the nucleation of the copper hydroxysulfates micro/nanostructures begins in the presence of SO_4^{2-}. This gives rise to an increase in mass and a corresponding sharp increase in R_{inst}. SEM micrographs recorded of the structures formed at this stage of growth show the simple bone-shaped stick (Figure 4, micrograph 4a). As the current passes through a maximum value (at ~200 s) other sticks start forming at the nucleation site (Figure 4, micrograph 4b). This indicates that this current is associated with the growth from overlapping nuclei. In the fourth stage, the current starts decreasing due to the superposition of the diffusion layers of the growing nuclei. Correspondingly, the mass increase starts to slow down giving a R_{inst} almost constant at around 1.323 mg/C. During this stage that lasts about 200 s, the sticks have grown in number and size to form hierarchical clusters which are not yet completely developed (Figure 4, micrograph 4c). The fifth and last stage is characterized by a monotonic decrease of current and a linear increase in mass with a rate (slope) slightly lower than the previous stage. In the meantime the R_{inst} has shifted to a lower value of 1.161 mg/C. This change could be due to the reciprocal hindrance that each cluster is now experiencing from the surrounding ones. Charge is being consumed to carry out the electrochemical reactions, such as oxygen reduction, but it has become more difficult to produce the necessary local concentration of ions to cause precipitation. At this final stage the hierarchical copper-based micro/nanostructures take the form shown in Figure 6. Finally, with the further progression of the deposition fully grown micro/nanostructures are formed.

CONCLUSIONS

Studies on the effect of the electrode potential on the deposition of copper-based materials onto PPy−PSS film showed that this has a major influence on the composition and morphology of the deposited materials. Hybrid microstructures were prepared by a simple two-step procedure comprising of two depositions at potentials of −0.10 and 0.10 V vs SCE, respectively. The SEM micrographs of the different stages of formation of the hierarchical micro/nanostructures at 0.10 V vs SCE on PPy−PSS films surface showed that the structures are formed from nanoparticles. The nanoparticles are aligned along nanowires that are then arranged into layered nanothin sheets. The nanosheets are then arranged concentrically to each other to finally form the hierarchical clusters. The nucleation is progressive and characterized by different stages of growth. It can be concluded that an electrode modified with a PPy−PSS film is a

novel, inexpensive, and simple tool useful for the deposition and fabrication of micro/nanomaterials with a range of shapes and compositions.

AUTHOR INFORMATION

Corresponding Author
*E-mail: chemistry.department@nuim.ie. Tel.: +353-1-7083770. Fax: +353-1-7083815.

REFERENCES

(1) Klein, J. D.; Herrick, R. D.; Palmer, D.; Sailor, M. J.; Brumlik, C. J.; Martin, C. R. *Chem. Mater.* **1993**, *5*, 902–904.
(2) Routkevitch, D.; Bigioni, T.; Moskovits, M.; Xu, J. M. *J. Phys. Chem.* **1996**, *100*, 14037–14047.
(3) Zhang, X. Y.; Zhang, L. D.; Chen, W.; Meng, G. W.; Zheng, M. J.; Zhao, L. X. *Chem. Mater.* **2001**, *13*, 2511–2515.
(4) Jin, C. G.; Xiang, X. Q.; Jia, C.; Liu, W. F.; Cai, W. L.; Yao, L. Z.; Li, X. G. *J. Phys. Chem. B* **2004**, *108*, 1844–1847.
(5) Fu, M. X.; Chen, F.; Zhang, J. X.; Shi, G. Q. *J. Mater. Chem.* **2002**, *12*, 2331–2333.
(6) Aizawa, M.; Shinohara, H.; Yamada, T.; Akagi, K.; Shirakawa, H. *Synth. Met.* **1987**, *18*, 711–714.
(7) Kuila, B. K.; Stamm, M. *J. Mater. Chem.* **2010**, *20*, 6086–6094.
(8) Zhu, S. M.; Gu, J. J.; Chen, Z. X.; Dong, J. P.; Liu, X. Y.; Chen, C. X.; Zhang, D. *J. Mater. Chem.* **2010**, *20*, 5123–5128.
(9) Wei, D.; Baral, J. K.; Osterbacka, R.; Ivaska, A. *J. Mater. Chem.* **2008**, *18*, 1853–1857.
(10) Wu, M. Q.; Snook, G. A.; Gupta, V.; Shaffer, M.; Fray, D. J.; Chen, G. Z. *J. Mater. Chem.* **2005**, *15*, 2297–2303.
(11) Ouyang, M.; Bai, R.; Xu, Y.; Zhang, C.; Ma, C. A.; Wang, M.; Chen, H. Z. *Trans. Nonferrous Met. Soc. China* **2009**, *19*, 1572–1577.
(12) Sun, L.; Chien, C. L.; Searson, P. C. *Chem. Mater.* **2004**, *16*, 3125–3129.
(13) El-Giar, E. M.; Said, R. A.; Bridges; Thomson, D. J. *J. Electrochem. Soc.* **2000**, *147*, 586–591.
(14) Musa, A. O.; Akomolafe, T.; Carter, M. J. *Sol. Energy Mater. Sol. Cells* **1998**, *51*, 305–316.
(15) Singh, D. P.; Neti, N. R.; Sinha, A. S. K.; Srivastava, O. N. *J. Phys. Chem. C* **2007**, *111*, 1638–1645.

20082

dx.doi.org/10.1021/jp204092x |*J. Phys. Chem. C* 2011, 115, 20076–20083

(16) Wang, C.; Yin, L.; Zhang, L.; Xiang, D.; Gao, R. *Sensors* **2010**, *10*, 2088–2106.

(17) Shishiyanu, S. T.; Shishiyanu, T. S.; Lupan, O. I. *Sens. Actuators, B* **2006**, *113*, 468–476.

(18) Poizot, P.; Laruelle, S.; Grugeon, S.; Dupont, L.; Tarascon, J. M. *Nature* **2000**, *407*, 496–499.

(19) Liu, W.; Chen, G.; He, G.; Zhang, W. *J. Nanopart. Res.* **2011**, *13*, 2705–2713.

(20) Allam, N. K.; Grimes, C. A. *Mater. Lett.* **2011**, *65*, 1949–1955.

(21) Siegfried, M. J.; Choi, K. S. *Adv. Mater.* **2004**, *16*, 1743–1746.

(22) Siegfried, M. J.; Choi, K. S. *Angew. Chem., Int. Ed.* **2005**, *44*, 3218–3223.

(23) Siegfried, M. J.; Choi, K. S. *Angew. Chem., Int. Ed.* **2008**, *47*, 368–372.

(24) Daltin, A. L.; Addad, A.; Baudart, P.; Chopart, J. P. *CrystEngComm* **2011**, *13*, 3373–3377.

(25) Daltin, A. L.; Chopart, J. P. *Cryst. Growth Des.* **2010**, *10*, 2267–2271.

(26) Lakes, R. *Nature* **1993**, *361*, 511–515.

(27) Courty, A. In *Nanomaterials and Nanochemistry*; Bréchignac, C., Houdy, P., Lahmani, M., Eds.; Springer: Berlin, 2008.

(28) Wolf, E. L. *Nanophysics and Nanotechnology: An Introduction to Modern Concepts in Nanoscience*; John Wiley & Sons: Weinheim, 2006.

(29) Filanovsky, B.; Granot, E.; Dirawi, R.; Presman, I.; Kuras, I.; Patolsky, F. *Nano Lett.* **2011**, *11*, 1727–1732.

(30) Xiang, J. Y.; Tu, J. P.; Qiao, Y. Q.; Wang, X. L.; Zhong, J.; Zhang, D.; Gu, C. D. *J. Phys. Chem. C* **2011**, *115*, 2505–2513.

(31) Xia, C.; Cai, X.; Ning, W.; Lin, G. *Anal. Chim. Acta* **2011**, *691*, 43–47.

(32) Reddy, N. K.; Devika, M.; Shpaisman, N.; Ben-Ishai, M.; Patolsky, F. *J. Mater. Chem.* **2011**, *21*, 3858–3864.

(33) Hang, T.; Hu, A.; Ling, H.; Li, M.; Mao, D. *Appl. Surf. Sci.* **2010**, *256*, 2400–2404.

(34) Li, Y.; Tan, B.; Wu, Y. *Nano Lett.* **2008**, *8*, 265–270.

(35) Feng, L.; Li, S. H.; Li, Y. S.; Li, H. J.; Zhang, L. J.; Zhai, J.; Song, Y. L.; Liu, B. Q.; Jiang, L.; Zhu, D. B. *Adv. Mater.* **2002**, *14*, 1857–1860.

(36) Guo, Z. G.; Fang, J.; Hao, J. C.; Liang, Y. M.; Liu, W. M. *ChemPhysChem* **2006**, *7*, 1674–1677.

(37) Andreoli, E.; Rooney, A. D.; Redington, W.; Gunning, R.; Breslin, C. B. *J. Phys. Chem. C* **2011**, *115*, 8725–8734.

(38) Andreoli, E.; Annibaldi, V.; Rooney, A. D.; Liao, K. S.; Alley, J. N.; Curran, S. A.; Breslin, C. B. *Electroanalysis* **2011**, *23*, 2164–2173.

(39) Holzhauser, P.; Bouzek, K. *J. Appl. Electrochem.* **2006**, *36*, 703–710.

(40) Ghijsen, J.; Tjeng, L. H.; van Elp, J.; Eskes, H.; Westerink, J.; Sawatzky, G. A.; Czyzyk, M. T. *Phys. Rev. B* **1988**, *38*, 11322–11330.

(41) Feser, R. Uniform Corrosion of Metals in Acid, Neutral and Alkaline Electrolytes. In *Encyclopedia of Electrochemistry*; Bard, A. J., Stratmann, M., Frankel, G. S., Eds.; Wiley: Hoboken, NJ, 2007; Vol. 4, p 99.

(42) Chavez, K. L.; Hess, D. W. *J. Electrochem. Soc.* **2001**, *148*, G640–G643.

(43) Yin, M.; Wu, C. K.; Lou, Y.; Burda, C.; Koberstein, J. T.; Zhu, Y.; O'Brien, S. *J. Am. Chem. Soc.* **2005**, *127*, 9506–9511.

(44) Zhou, Y. C.; Switzer, J. A. *Scr. Mater.* **1998**, *38*, 1731–1738.

(45) Wang, Z. L. *J. Phys. Chem. B* **2000**, *104*, 1153–1175.

(46) Li, D. D.; Chien, C. J.; Deora, S.; Chang, P. C.; Moulin, E.; Lu, J. G. *Chem. Phys. Lett.* **2011**, *501*, 446–450.

(47) Cui, J.; Gibson, U. J. *J. Phys. Chem. C* **2010**, *114*, 6408–6412.

(48) Musselman, K. P.; Wisnet, A.; Iza, D. C.; Hesse, H. C.; Scheu, C.; MacManus-Driscoll, J. L.; Schmidt-Mende, L. *Adv. Mater.* **2010**, *22*, E254–E258.

(49) McShane, C. M.; Siripala, W. P.; Choi, K. S. *J. Phys. Chem. Lett.* **2010**, *1*, 2666–2670. 19 Eranna, G.; Joshi, B. C.; Runthala, D. P.; Gupta, R. P. *Crit. Rev. Solid State Mater. Sci.* **2004**, *29*, 111–188.

(50) Eranna, G.; Joshi, B. C.; Runthala, D. P.; Gupta, R. P. *Crit. Rev. Solid State Mater. Sci.* **2004**, *29*, 111–188.

(51) Singh, D. P.; Neti, N. R.; Sinha, A. S. K.; Srivastava, O. N. *J. Phys. Chem. C* **2007**, *111*, 1638–1645.

(52) Lin, G.; Jia, W.; Lu, W.; Jiang, L. *J. Colloid Interface Sci.* **2011**, *353*, 392–397.

(53) Dunitz, J. D.; Bernstein, J. *Acc. Chem. Res.* **1995**, *28*, 193–200.

(54) Yang, R.; Naoi, K.; Evans, D. F.; Smyrl, W. H.; Hendrickson, W. A. *Langmuir* **1991**, *7*, 556–558.

(55) Scharifker, B.; Hills, G. *Electrochim. Acta* **1983**, *28*, 879–889.

(56) Eliaz, N.; Eliyahu, M. *J. Biomed. Mater. Res., Part A* **2007**, *80A*, 621–634.